Sonar Signal-Gain Limits from Internal Waves

MITRE

Sonar Signal-Gain Limits from Internal Waves

Stanley M. Flatté

October 1998

JSR-97-211

JASON
The MITRE Corporation
1820 Dolley Madison Boulevard
McLean, Virginia 22102-3481
(703) 883-6997

REPORT DOCUMENTATION PAGE

Form Approved
OMB No. 0704-0188

1. AGENCY USE ONLY (Leave blank)	2. REPORT DATE	3. REPORT TYPE AND DATES COVERED
	October 27, 1998	

4. TITLE AND SUBTITLE

Sonar Signal-Gain Limits from Internal Waves

5. FUNDING NUMBERS

13-988534-A1

6. AUTHOR(S)

S. Flatte'

7. PERFORMING ORGANIZATION NAME(S) AND ADDRESS(ES)

The MITRE Corporation
JASON Program Office
1820 Dolley Madison Blvd
McLean, Virginia 22102

8. PERFORMING ORGANIZATION REPORT NUMBER

JSR-97-211

9. SPONSORING/MONITORING AGENCY NAME(S) AND ADDRESS(ES)

Department of the Navy
Office of the Chief of Naval Operations
2000 Navy Pentagon
Washington, DC 20350-2000

10. SPONSORING/MONITORING AGENCY REPORT NUMBER

JSR-97-211

11. SUPPLEMENTARY NOTES

12a. DISTRIBUTION/AVAILABILITY STATEMENT

Approved for public release; distribution unlimited.

12b. DISTRIBUTION CODE

Distribution Statement A

13. ABSTRACT *(Maximum 200 words)*

This report will present the state of knowledge of internal-wave effects from the point of view of low-frequency sonar systems, and will make recommendations to the sonar-system designer and operator as to when to expect internal-wave effects to become important. It will also explain where oceanographic measurement and analysis are needed to determine the limits on sonar-system design and performance that are due to internal waves.

The calculations in this report are based on the universal Garrett-Munk spectrum, with differences in different parts of the ocean arising from the behavior of different water masses.

14. SUBJECT TERMS

15. NUMBER OF PAGES

16. PRICE CODE

17. SECURITY CLASSIFICATION OF REPORT	18. SECURITY CLASSIFICATION OF THIS PAGE	19. SECURITY CLASSIFICATION OF ABSTRACT	20. LIMITATION OF ABSTRACT
Unclassified	Unclassified	Unclassified	SAR

Contents

List of Figures

1 INTRODUCTION

Over the past twenty years, it has become clear that limits on performance of low-frequency sonar-systems from oceanographic variability are measurable, and that internal waves are a major contributor to these limits. However, in deep water these limits have been so weak that sonar systems in the field have not been built of a size and type that would be affected by decoherence due to internal waves.

Two changes in the situation suggest a re-investigation of the limits due to internal waves. First, target submarines have gotten quieter, so that larger and more ambitious sonar systems with higher gain are being contemplated. Second, shallow-water, coastal regions are taking on a higher level of importance in operational considerations. Both of these changes move internal-wave effects into a more significant position.

This report will present the state of knowledge of internal-wave effects from the point of view of low-frequency sonar systems, and will make recommendations to the sonar-system designer and operator as to when to expect internal-wave effects to become important. It will also explain where oceanographic measurement and analysis are needed to determine the limits on sonar-system design and performance that are due to internal waves.

The calculations in this report are based on the universal Garrett-Munk spectrum, with differences in different parts of the ocean arising from the behavior of different water masses. Although different strengths of the internal-wave field are easily taken into account, if the internal-wave field is significantly different from the GM model, these calculations will not be accurate. This particularly may be the case in some shallow-water locations. Furthermore, other effects such as solitons, solibores, or intrusions may be important in some locations. Nevertheless, we feel that it is worthwhile doing the GM

calculation as a reference from which to judge any alternative models that may arise in the future.

The effectiveness of internal waves in causing acoustic fluctuations is dependent on oceanographic behavior (the temperature-salinity (T-S) relation) whose systematics would need to be established more precisely than is known at present. It is also dependent on the local strength of internal waves, whose variability is known to exist, but whose systematics need to be established also. Finally it is dependent on the local sound-speed profile, which needs to be locally measured, and the buoyancy-frequency profile, which needs to be at least modelled reasonably precisely.

A Scenario

Imagine that a sonar system is built that has 10^5 hydrophones in it, and that it is deployed near a coast in 1000 meters of water. Without oceanographic variability, such a system is capable of 50 dB of signal gain against isotropic noise. At 100 Hz it would have an aperture of 1000 m in the vertical and about 6 km in the horizontal. The calculations in this report will show that at a range of 500 km, a reference internal-wave model will predict acoustic coherence lengths that vary widely between ocean regions, but with typical values of 5000 m in the vertical and 25 km in the horizontal. Thus it would appear that a sonar-system designer is justified in ignoring internal-wave effects.

However, in our scenario, we happen to be in the North Polar Pacific (near Japan), and a nearby storm has been raging for a week or so. As a result, we are in an acoustically sensitive region, and the internal-wave strength has gone up by a factor of ten in energy (displacements have increased by a factor of three). The internal-wave-induced coherence lengths drop by a factor of ten to 500 m and 2.5 km, and the gain drops below the ideal 50 dB by about 6 dB (at 500 km). In addition, the sonar system has been relying on some incoherent time integration, and the gain available has dropped also.

As a result, a quiet target has dropped below threshold and is now invisible.

As a modification of our scenario, we move in toward shallower water, say 200-m depth, but we consider ranges of 20 km instead of 500 km. Internal waves will not limit the vertical coherence, because the water depth is so small; we assume coherence up to the maximum of 200 m in the vertical. Horizontal coherence lengths in the standard model are in the hundreds of kilometers, so that no internal-wave effects are significant.

This kind of analysis is the starting point for evaluating the actual limits imposed by internal waves. It seems clear that internal-wave effects should be considered first in the long-range, deep-water scenario, and that shallow-water scenarios at low frequency that have internal-wave effects will be much rarer, involving special cases. The long-range signal-gain limits due to internal waves are going to be in the regime of 50 dB, with a more exact prediction requiring the monitoring of internal-wave strength as a function of geographical location and time, in addition to already-realized monitoring requirements on the sound-speed and buoyancy-frequency profiles. Thus, knowledge of the effectiveness of a sonar system that is large enough to be affected by internal waves will require:

- monitoring the local sound-speed profile (already done).
- knowing the local T-S relation in an acoustically relevant manner.
- monitoring the local buoyancy-frequency profile.
- monitoring the local strength of internal waves.

The rest of this report will describe our present knowledge of all these factors, and how they enter into sonar-system performance.

2 OCEAN CHARACTERIZATION

2.1 Sound Speed and Buoyancy Frequency

In order to make a realistic prediction of acoustic behavior, including the effects of internal waves, it is necessary to use realistic profiles with depth of the sound speed and buoyancy frequency. Such profiles can be obtained from a well-known database that has been compiled under the name of Levitus. This database has information on temperature and salinity as a function of depth for each season and on a one-degree grid of latitude and longitude. Information is provided every ten meters in depth down to 1500 m. There is also a yearly average database, called "annual", which includes information down to the depth of the ocean, which is in most places between 4000 and 6000 m.

In order to develop realistic profiles that represent a large ocean region, such as the North Pacific, we can pick a particular latitude (say 30N) and average the profiles over longitude (say 140W-200W). However, it turns out that this is a dangerous and unreliable procedure, because the act of averaging the sound-speed profile and the buoyancy profile separately can generate two profiles that are unrepresentative in important ways. Therefore it is better to look at the profiles of the different longitudes separately and pick a particular longitude that is "representative".

The representative geographical locations we have picked for each of a number of ocean regions are shown in Table 1. The sound-speed and buoyancy profiles from the Levitus database that correspond to these representative locations are shown in Figure 1.

Table 1: Ocean regions chosen for this study.

Ocean Region	Latitude	Longitude
North Polar Atlantic	$60°N$	$40°W$
North Polar Pacific	$50°N$	$180°W$
North Atlantic	$30°N$	$30°W$
North Pacific	$30°N$	$175°W$
Equatorial Atlantic	$0°$	$25°W$
Equatorial Pacific	$0°$	$150°W$
Equatorial Indian	$0°$	$90°E$
South Atlantic	$30°S$	$15°W$
South Pacific	$30°S$	$135°W$
South Indian	$30°S$	$75°E$
South Polar Atlantic	$60°S$	$20°W$
South Polar Indian	$60°S$	$120°E$

The sound-speed profile will control the deterministic part of the behavior of acoustic propagation in the ocean region being considered. The North Atlantic has a considerably weaker thermocline than the other regions, and of course the polar regions have almost no thermocline, instead maintaining a reverse gradient for depths almost all the way to the surface.

The buoyancy-frequency profile will be needed for predicting the effects of internal waves. It varies in the upper ocean by factors of order five between different ocean basins, and this factor will have dramatic effects on internal-wave acoustic effects.

2.2 Internal-Wave Spectrum and Strength (ζ_o^2)

Deep-water internal waves are characterized reasonably well by their power spectrum, which has been empirically determined by Garrett and Munk (GM) to be expressible as factorizable in frequency and vertical mode

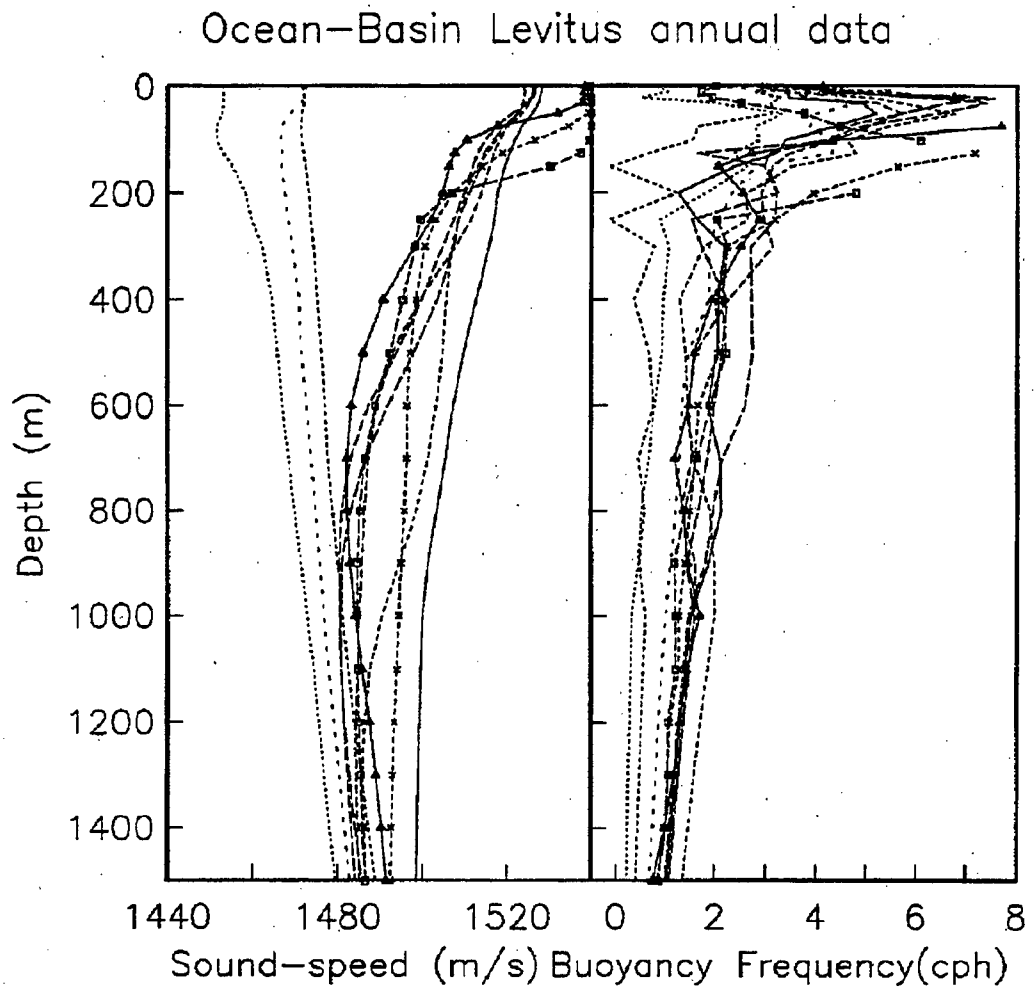

Figure 1: The profiles of sound speed and buoyancy frequency, for the ocean regions used in this study, from the Levitus annual database. The various profiles are listed from longest to shortest dash (solid line first): North Atlantic, South Atlantic, North Pacific, South Pacific, South Indian, North Polar Atlantic, South Polar Atlantic, South Polar Indian.

number:[1]

$$S(j,\omega) = \langle \zeta^2(z) \rangle \cdot \frac{N_j}{j^2 + j_*^2} \cdot \frac{N_\omega \omega_i (\omega^2 - \omega_i^2)^{1/2}}{\omega^3} \qquad (2\text{-}1)$$

where N_j and N_ω are normalization constants defined in Flatté and Esswein,[2] such that the sum over j and integral over ω of the spectrum gives $\langle \zeta^2(z) \rangle$.

Later, the dispersion relation of internal waves relating wavevector $\vec{k}$ to mode number j and frequency ω will be needed. Define k as the magnitude of the horizontal component of the wavevector: $k = \sqrt{k_x^2 + k_y^2}$. The vertical wavevector component is k_v and the frequency is ω.

$$k = \alpha j (\omega^2 - \omega_i^2)^{1/2}; \quad k_v = \alpha j n_e. \qquad (2\text{-}2)$$

The quantity α depends on the vertical profile of buoyancy frequency $n(z)$, and is approximately given by:

$$\alpha^{-1} = \frac{1}{\pi} \int_0^D n(z) dz \qquad (2\text{-}3)$$

where D is the depth of the ocean. This integral of the buoyancy-frequency profile will be an important parameter in determining the acoustic effects of internal waves. The value of α^{-1} for the deep ocean is typically between 3 and 5 cph-km, or in other units, 5 to 9 m s^{-1}. Its value in shallow water can be estimated by using a depth of 200 m and a buoyancy frequency of 8 cph, which gives 1.6 cph-km, or 3 m s^{-1}. Thus internal waves in 200 m of water move at speeds that typically are only 2 or 3 times slower than the speed of internal waves in deep water.

The quantity ζ in Equation (2-1) is the displacement of internal waves at a particular depth; it is related to the energy density of internal waves and to the buoyancy profile. It has been determined by measurements that $\langle \zeta^2(z) \rangle$ is near 50 m^2 at depths in the deep ocean at which the buoyancy frequency is 3 cph. Let ζ_o^2 be this reference level, with an accompanying definition of n_o as 3 cph. However, there are substantial variations from this "reference" level. These variations are of great interest to oceanographers, because they

represent the sources and sinks of the internal wave field. They are also of great interest to the sonar-system designer, because the acoustic effects of internal waves will be proportional (in some sense) to the internal-wave strength.

2.2.1 The Equator Problem

Here we mention a difficulty in the definition of the GM spectrum. The expressions for most quantities depend on the inertial frequency, which goes to zero at the equator. Therefore, the frequency dependence of the internal-wave displacement spectrum is singular at the equator. There is no agreed-upon simple modification of the GM spectrum that avoids this problem, although the physics of the various kinds of waves that are involved (Kelvin, Rossby, etc) is well known. Until a simple GM modification for equatorial regions is available, the sonar-system designer has little guidance in this area.

2.3 Ratio of Sound-Speed to Buoyancy Effects (F)

Even if the internal-wave reference displacement ζ_o applied universally to the world's oceans, the acoustic effects due to internal waves would vary from ocean basin to ocean basin. This is because different ocean basins have different *water masses*. That is, different ocean basins have different temperature-salinity relations. Acoustic effects of internal waves depend on the product of potential sound-speed gradient and internal-wave displacement, while internal-wave strength depends on the product of density gradient and internal-wave displacement. Let us call F the ratio of acoustic effect to internal-wave effect:

$$F = \frac{\Delta C_p / C_p}{\Delta \rho / \rho} \tag{2-4}$$

where C_p is the potential sound speed (that is, the sound speed with the pressure effect removed). Both potential sound speed and density depend on temperature, salinity, and pressure, according to the equation of state of seawater. There are well-known formulas for these quantities, based on extensive measurements in the laboratory: notably, the results of Chen and Millero [3] for density and Del Grosso [4] for sound speed. In order to use these results, the temperature-salinity characteristics of ocean basins must be oceanographically understood.

2.3.1 Water Masses

Different ocean regions have different temperature-salinity (TS) relations, which to first order are independent of time (including season). Figure 2 shows the TS relations for twelve ocean basins by plotting S vs T for a particular latitude and ocean basin, with each plot having several different longitudes. It is seen that the different longitudes fall closely on each other over a substantial depth region. Although it isn't shown in the plots, the depth below which the different longitudes are quite similar is about 200 meters. Above that depth, the seasonal heating of the sun imposes substantial differences.

If the plots of salinity or temperature were presented as functions of depth, there would be much more difference between different longitudes. By presenting the results in terms of S and T, the oceanographers have thus been able to identify (by ocean basin and depth region) different water masses that change very little over the years. Each of the curves of salinity versus temperature can be used to determine the F factor as a function of temperature.

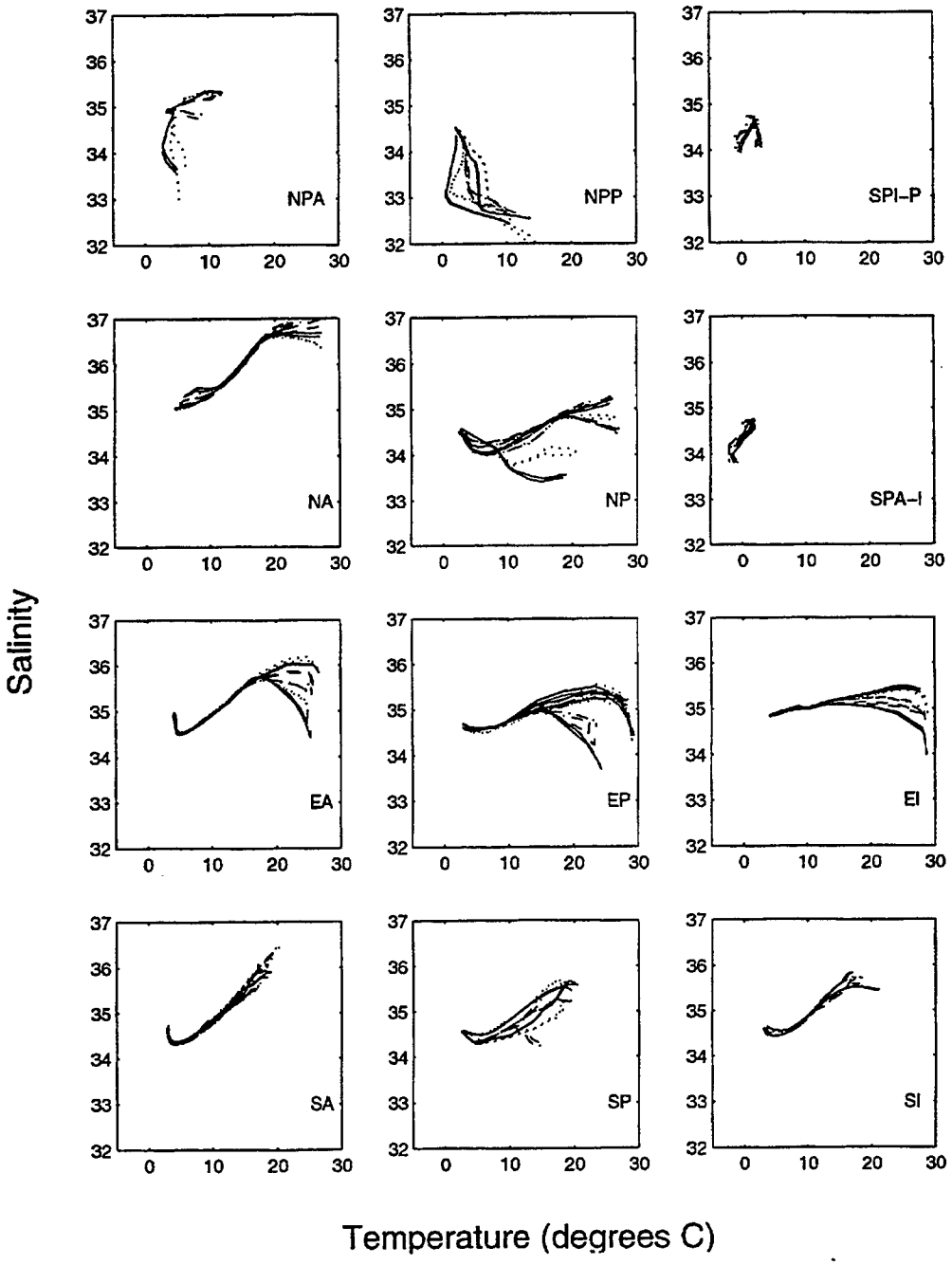

Figure 2: Temperature-Salinity (TS) plots for twelve ocean regions used in this study.

A summary plot of TS relations for different ocean basins is shown in Figure 3, where representative longitudes from the previous figures have been chosen.

2.3.2 Results for F

It is tempting to start by approximating the equation of state of seawater by first derivative terms,[5] but that turns out to be inadequate in this situation. (The points in the Levitus database are too far apart to use first derivatives, and the coefficients of the first-derivative terms are too variable with temperature and depth.) For the results shown here, the complete formulas have been used. Figure 4 shows F as a function of depth for a number of ocean regions. It is seen that F varies over a factor of three, and that will have dramatic effects on the relative acoustic effects of internal waves in different oceans. Because different seasons and latitudes have different temperatures at the same depth, the value of F varies over longitude and season. However, if F is plotted as a function of temperature, the underlying water-mass characteristic of the ocean basin is revealed more clearly by a narrowing of the F curves. Figure 5 shows F as a function of temperature for a number of ocean regions, and Figure 6 shows F for representative longitudes from each of those ocean regions. Again we see the variation of F over a factor of three.

2.4 Shallow-Water Modifications

Internal waves in shallow water are the subject of on-going research. However, for the sonar-system designer, and the oceanographic-experiment designer, it is important to have a qualitative picture of the shallow-water situation. Measurements of internal waves in water with depths down to

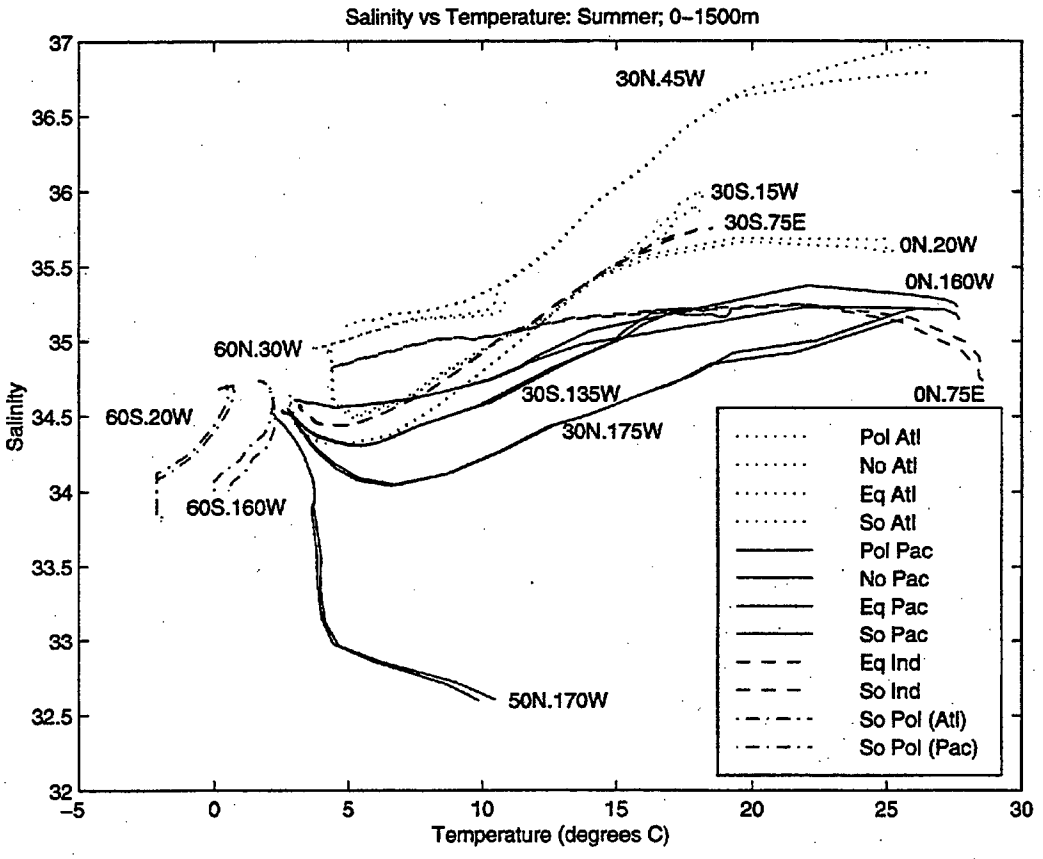

Figure 3: Temperature-Salinity (TS) summary plot for the twelve ocean regions used in this study.

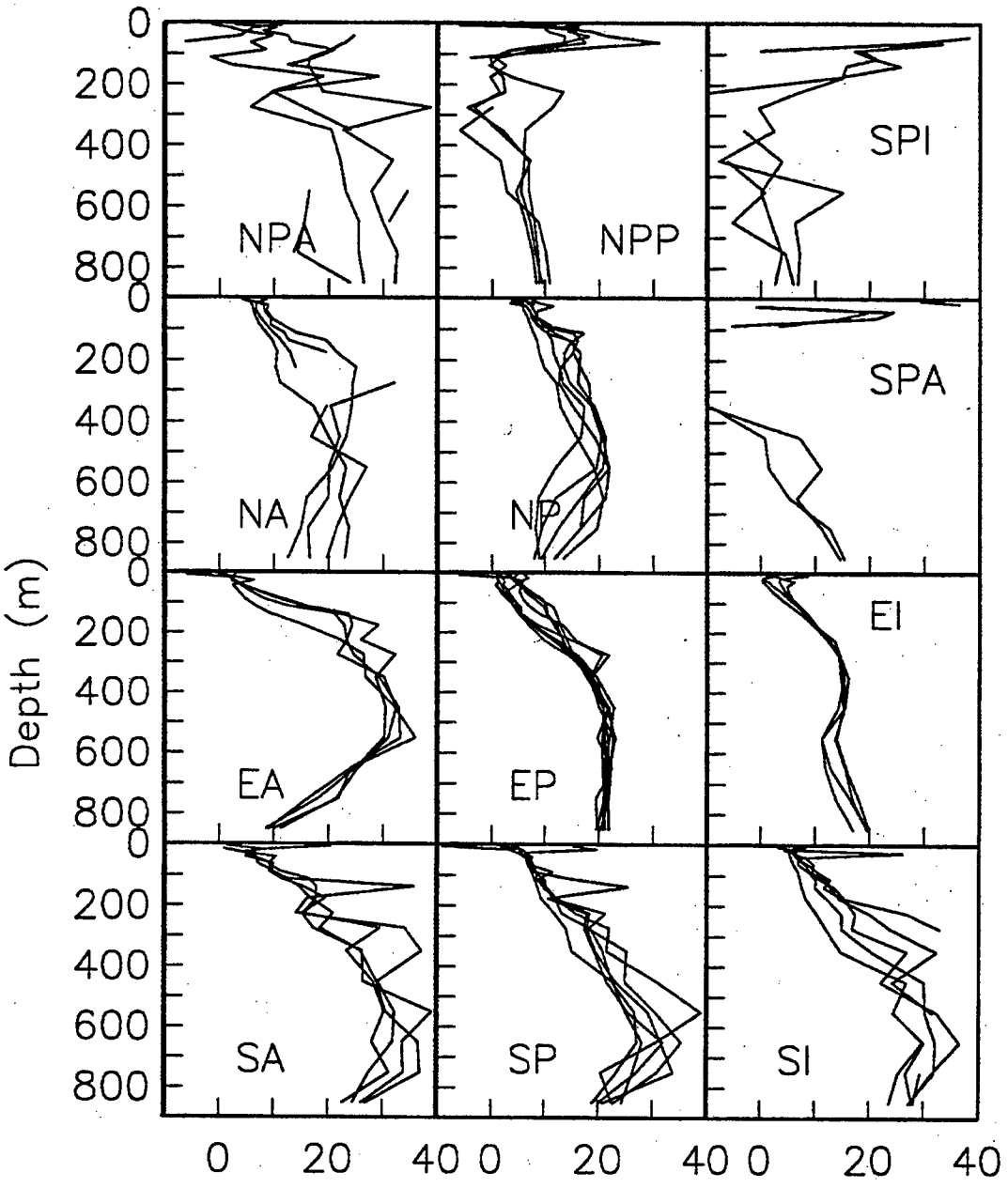

Figure 4: Acoustic-effect factor F as a function of depth for twelve ocean regions. This factor is the ratio of fractional sound-speed variation to the fractional density variation due to an internal wave. The different curves on each plot are for different longitudes.

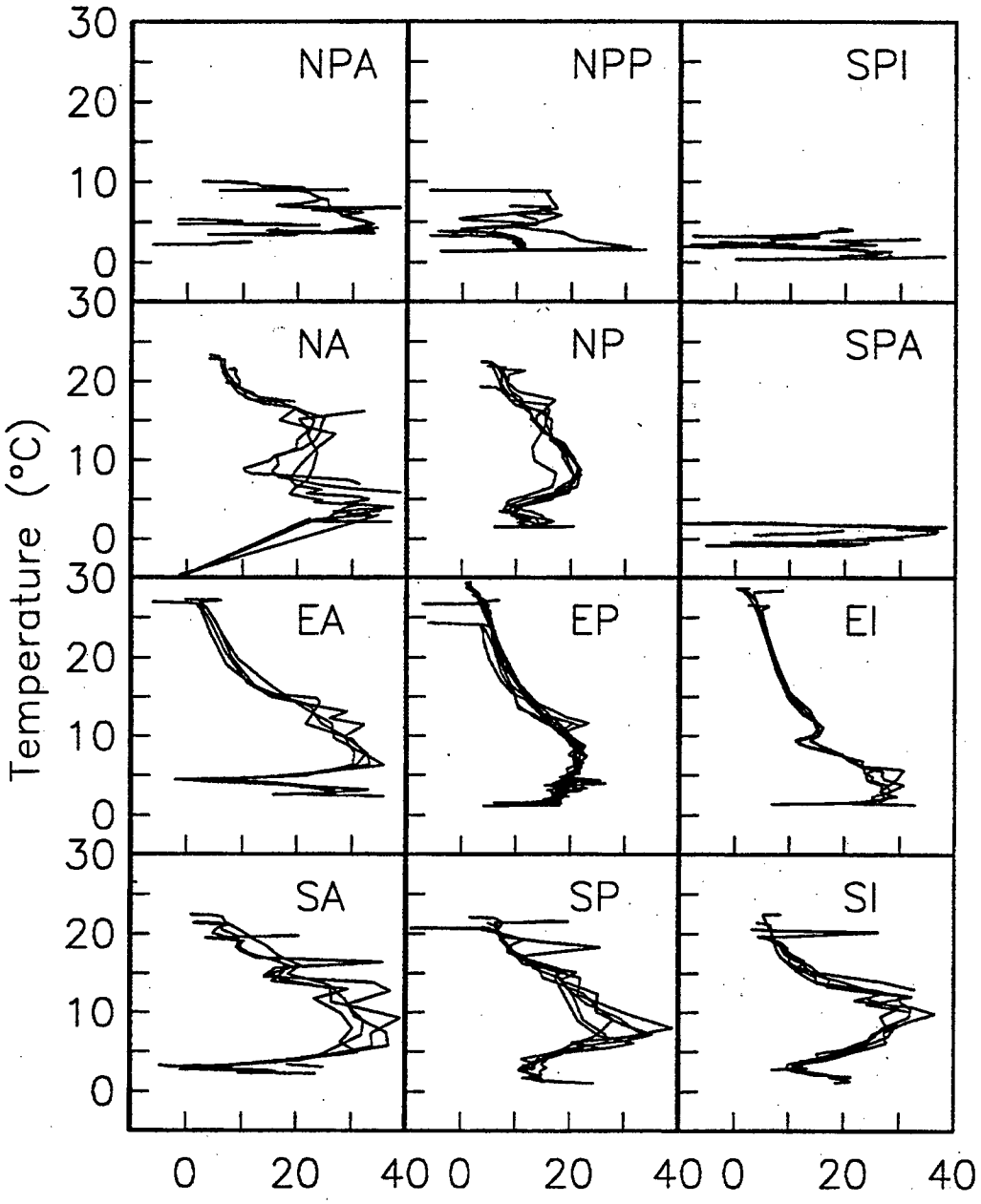

Figure 5: Acoustic-effect factor F as a function of temperature for twelve ocean regions. This factor is the ratio of fractional sound-speed variation to the fractional density variation due to an internal wave. The different curves on each plot are for different longitudes.

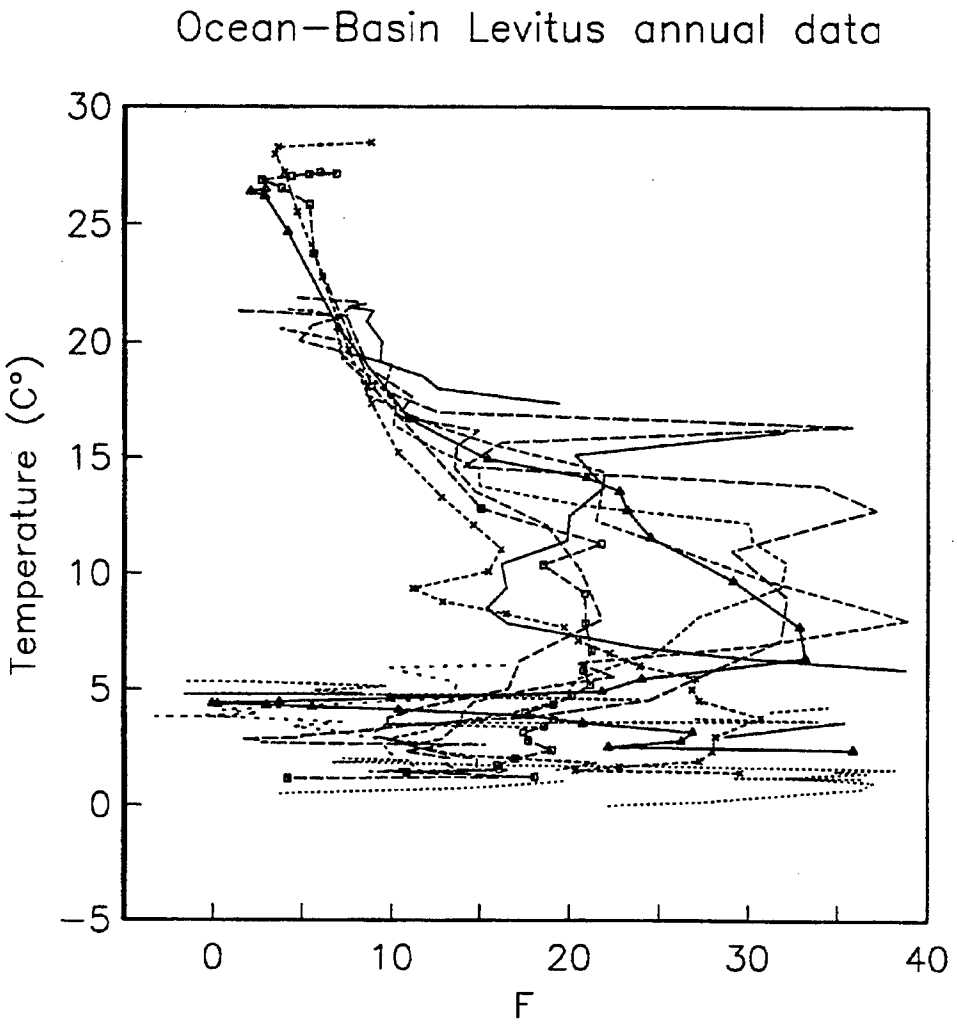

Figure 6: Acoustic-effect factor F as a function of temperature for the ocean regions used in this study. The various profiles are listed from longest to shortest dash (solid line first): North Atlantic, South Atlantic, North Pacific, South Pacific, South Indian, North Polar Atlantic, South Polar Atlantic, South Polar Indian.

100 meters have been made in a variety of areas; those measurements have shown that the GM spectrum is not an unreasonable model when a few modifications are taken into account. (The most recent measurements have been made off the East and West coasts of the United States.)

- In water of a few hundred meters depth the internal waves are vertically coherent to a high degree. This means that the vertical correlation length of internal waves is effectively the water depth. But in deep water the internal-wave vertical correlation length is about 200 meters. Since this is not far from the depth in shallow water, the GM model as it stands is not inappropriate.

- Observations in shallow water show internal-wave rms displacements of order 10 meters, just as in deep water. However, the buoyancy frequency in shallow water is systematically larger than in the surface waters of the deep ocean by about a factor of two (the difference between, say, 8 and 4 cph). This does not change the spectrum, but does affect the overall strength of internal-wave acoustic effects in a simple way.

- Shallow-water observations have identified internal waves other than the superposition of linear waves described by the GM spectrum. In particular, solitons and solibores are often observed.[6, 7] This study will not evaluate the effect of these other internal waves. However, the SWARM experiment shows an example in which the GM part of the spectrum has about the same rms displacement as the solitons, and since solitons have a much shorter correlation length along their direction of propagation, their effects on acoustics are often much less. When they are weak, as seems to be the case on the Pacific coast (Murray Levine, private communication, 1997), they have negligible effect. When they are strong, (e.g. in the SWARM data) their effects would be no more than comparable to GM effects in size, though their frequencies are much higher than GM internal waves. The sonar-system

designer is justified for the most part in keeping them in abeyance for the moment. When future research establishes systematic models for solitons and solibores that are comparable to the GM model, then sonar-system designers will be able to incorporate their effects.

A set of shallow-water locations around the world where a combination of political and military factors indicate the possible existence of future naval conflict are given in Table 2, along with their typical ocean-depth regimes.

Note that only the Falklands are in the Atlantic, or part of any "Atlantic Rim"! Only the Falklands and the related Strait of Magellan are in the Southern Hemisphere.

Table 2: Interesting shallow-water ocean regions.

Ocean Region	Latitude	Longitude	Depth Regime
Persian Gulf	$27°N$	$52°E$	30-90 m
Strait of Hormuz	$20°N$	$60°E$	30-90 m
Taiwan Strait	$25°N$	$120°E$	50-80 m
Strait of Malacca	$5°N$	$100°E$	40-1000 m
Molucca Sea	$0°$	$125°E$	1000-4000 m
Korea Strait	$35°N$	$130°E$	50-200 m
Panama Canal	$10°N$	$80°W$	30-1000 m
Strait of Magellan	$53°S$	$74°W$	30-500 m
The Falklands	$52°S$	$62°W$	60-500 m

2.5 Sound-Speed-Variance Depth Dependence

The effects of sound-speed variability in ocean "surface" waters (i.e. those waters within about 300 m of the surface) are important. The GM model was put together to apply to the "deep" ocean: i.e. waters at depths of 1000 m or more. At these large depths it is very useful to apply the WKBJ

approximation to internal-wave vertical wavefunctions. Yet the GM model has been remarkably useful for depths much closer to the surface. If it is applied all the way to the surface, the WKBJ approximate wavefunctions do not go to zero as the real internal-wave wavefunction must. Therefore a correction must be made to reduce the calculated effects of internal waves when the WKBJ approximations are used.[8]

Figure 7 shows the variance of sound-speed fluctuations in an internal-wave model in which the buoyancy frequency has a Munk canonical profile.[9] The WKBJ approximation is seen to increase from large depths all the way to the surface. A numerical simulation of internal waves with proper vertical mode functions results in a sound-speed variance that goes to zero at the surface, and an empirical function $m(z)$ has been developed to correct the WKBJ approximation to account for the numerical-simulation results:[8]

$$m(z) \;=\; 1 - e^{\frac{z}{z_1}} \tag{2-5}$$

where $z_1 = 55$ m. This empirical function has been shown to result in accurate predictions of internal-wave-induced sound-speed acoustic fluctuations for acoustic energy that travels near the ocean surface during part of its path.[8] This empirical function has been used in all the calculations in Section 3 of this report.

2.6 Internal-Wave Correlation Lengths

In the ray approximation, acoustic effects depend on the integral of sound-speed variations along the direction of propagation of a ray. Upon evaluation of such acoustic effects by a path-integral technique (see Section 3), a property of importance appears in the form of a correlation length along the ray, which has been called L_p.[5] For almost twenty years, formulas have been used for L_p that were presented by Munk and Zachariasen, based on approximating rays locally as straight lines.[10] Recently a generalization to

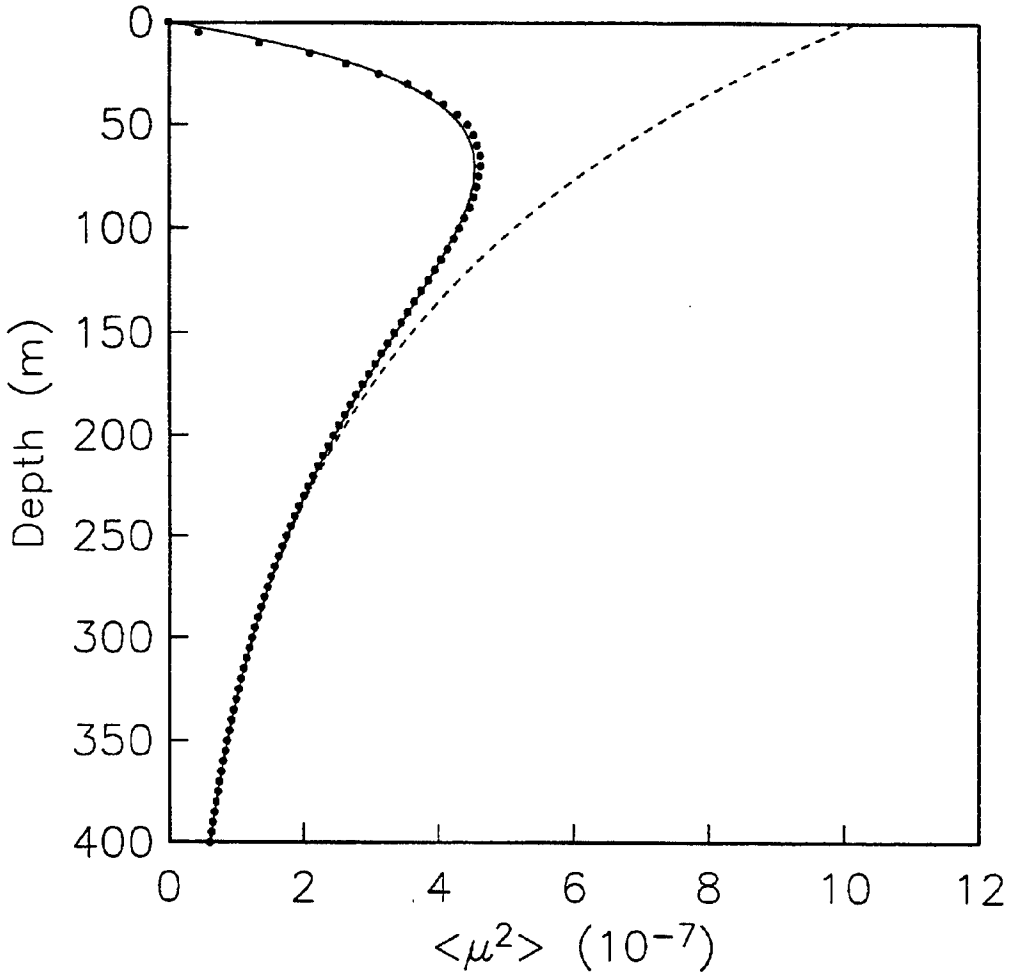

Figure 7: The internal-wave-induced sound-speed variance $\langle \mu^2 \rangle$ as a function of depth, for a case in which the profile of buoyancy frequency is canonical. The solid line is the analytic profile expected from an exponential buoyancy frequency and the WKBJ approximation. The dashed line is the result of numerical simulation of an internal-wave field with use of the GM spectrum, and with accurate mode wave functions calculated on the basis of the buoyancy-frequency profile. The dash-dot line is the WKBJ approximation corrected with an empirical function.

this approximation that accounts for ray curvature has been developed.[8]

The correlation length L_p can be defined in terms of two dimensionless parameters. The first parameter ρ_s is related to the anisotropy of the internal-wave spectrum:

$$\rho_s = \frac{n_s}{\omega_i} \tan\theta. \tag{2-6}$$

where n_s is the buoyancy frequency at the depth at which L_p is being evaluated, and θ is an angle with the horizontal at that depth.

An expression for L_p is then:

$$L_p = \frac{N_\omega}{\alpha\omega_i} \sum_j \frac{N_j}{j(j^2+j_*^2)} \int_0^\infty d\beta \left(\frac{n_e}{n_s}\right)^3 \cos(\beta\rho_s) F(\beta), \tag{2-7}$$

where

$$F(\beta) = 2\beta \int_0^\infty \frac{J_0(v) v^2 dv}{[v^2+\beta^2]^2} \tag{2-8}$$

and where n_e is an "effective" buoyancy frequency that applies to two points separated along an acoustic ray. The details of the derivation of this formula are presented in the reference; here it suffices to present the results as they are used in our calculations, and to say that if n_e/n_s is set to unity, the old straight-line approximation is recovered.

Note that $F(\beta)$ is defined such that

$$\int_0^\infty F(\beta) d\beta = 1 \tag{2-9}$$

The behavior of n_e/n_s is controlled by the depth behavior of two points on a ray trajectory symmetrically placed on either side of the evaluation point. and by the depth dependence of the buoyancy frequency. A series of approximations, assuming the ray trajectory to have constant curvature, results in the definition of another dimensionless parameter σ:

$$\sigma = \frac{3}{4Br\alpha^2\omega_i^2} \equiv \frac{r_I}{r} \tag{2-10}$$

where B is a scale length of the buoyancy-frequency profile: typically 1300 m. The parameter σ represents the ratio between an internal-wave length scale (r_I) and the ray radius of curvature (r). A typical value of r_I is 1500 km.

The result of all these definitions is a final expression for L_p in terms of dimensionless parameters:

$$L_p = \left(\frac{4Br_I}{3}\right)^{\frac{1}{2}} \sum_j \frac{N_\omega N_j}{j(j^2+j_*^2)} \int_0^\infty d\beta e^{-\frac{\sigma\beta^2}{2j^2}} \cos(\beta\rho_s) F(\beta), \qquad (2\text{-}11)$$

Figure 8 shows L_p as a function of ρ_s (corresponding to ray angle with the horizontal) evaluated for various values of σ (corresponding to curvature of the ray trajectory). The σ values are 0, 1, 10, 20, 50, 100, 200, and 500. The values of L_p for $\sigma \leq 1$ are reasonably close to those from the straight-line approximation. The values of L_p for more curved rays (larger σ) are more isotropic: smaller in the horizontal direction and larger for steep rays.

The results shown in Figure 8 were calculated numerically by tabulating $F(\beta)$. It is useful to find an analytic expression for L_p in order to make computer calculations more efficient. A useful expression has been found:[8]

$$L_p = L_{p0} \frac{\left[1 - \exp\left[-\left(\frac{\sigma_c}{\sigma}\right)^p\right]\right]^q}{1 + \left(\frac{\rho_s}{\rho_c}\right)^{q_a} \left(\frac{\sigma_c}{\sigma}\right)^{p_a}} \qquad (2\text{-}12)$$

where the values of the various parameters are: ρ_c=3.5, σ_c=0.0204, p=0.385, p_a=0.5, q=1.3, and q_a=2.0. The value of L_{p0} is given by:

$$L_{p0} = \left(\frac{4Br_I}{3}\right)^{\frac{1}{2}} N_\omega N_j M_j^{-1} \qquad (2\text{-}13)$$

where N_j, M_j, and N_ω are normalization constants defined in Flatté and Esswein.[2]

The above empirical formula applies for $\sigma > 6$. If $\sigma \leq 6$ then the formula is used with $\sigma = 6$. Figure 9 shows results from the analytic empirical formula for σ values of 0, 6, 10, 20, 50, 100, 200, and 500.

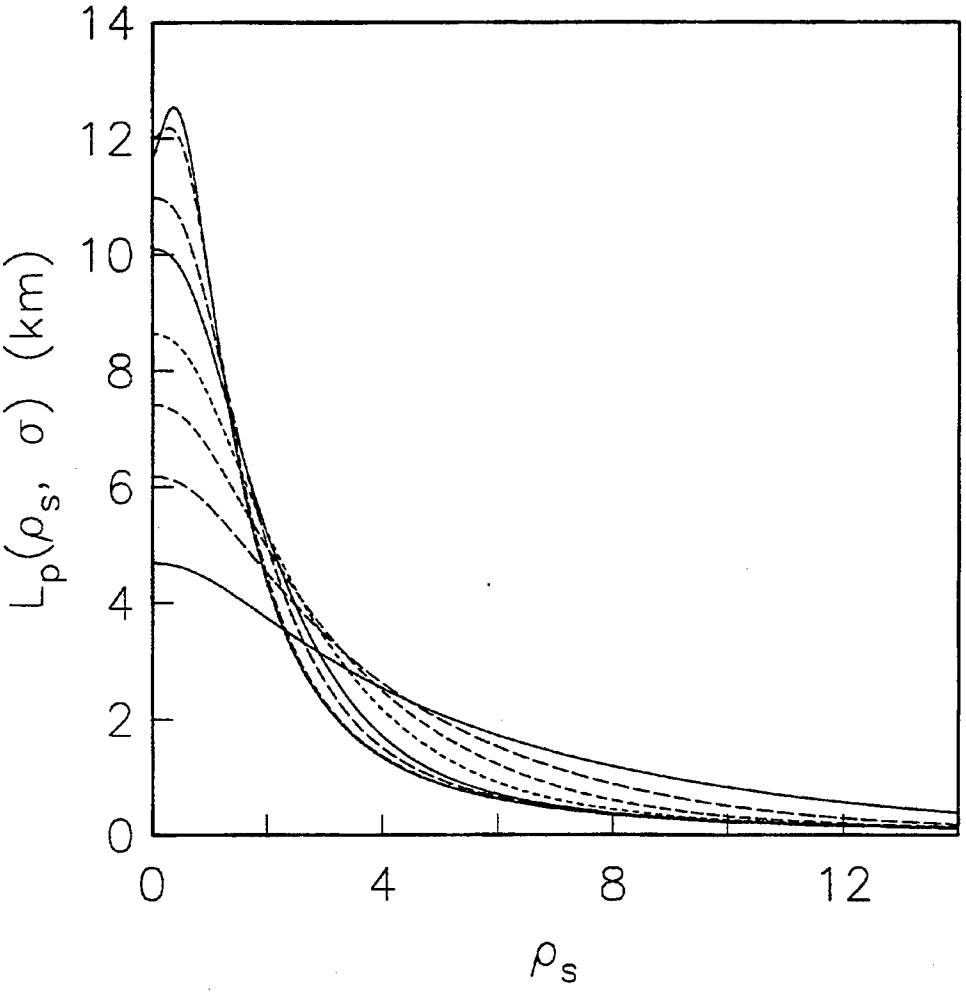

Figure 8: The internal-wave correlation length L_p as a function of the dimensionless parameter ρ_s, which represents the angle of the ray trajectory with the horizontal. Calculations have been made by numerical evaluation of $F(\beta)$.

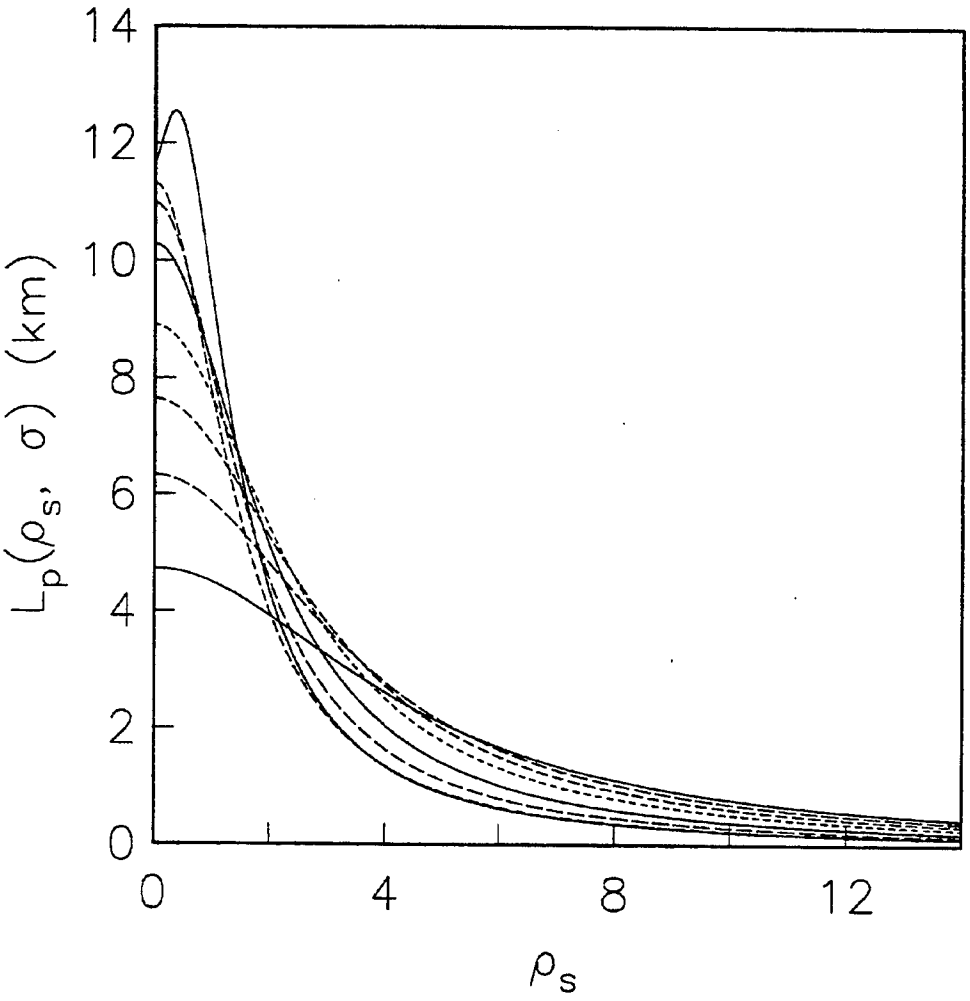

Figure 9: The internal-wave correlation length L_p as a function of the dimensionless parameter ρ_s. Calculations have been made with empirical analytic formulas.

Values of σ for ocean rays depend upon the sound-speed profile and the parameters characterizing the internal-wave field (r_I). Figure 10 shows two sets of profiles (for sound speed and buoyancy frequency) for conditions in the north Pacific. The first set corresponds to a canonical profile used in simulation of the SLICE89 experiment.[11] The second set is an average of profiles taken along a 3.2 Mm path between California and Hawaii for the ATOC experiment.[12] Figure 11 shows σ as a function of depth for the two profile sets in the north Pacific. The values of σ range up to 600, which corresponds to a ray radius of curvature of about 2 km.

2.7 Geographical and Seasonal Variations - The Systematic View (F vs ζ_o^2)

In order to predict the effects of internal waves on acoustic propagation, a reasonable pair of sound-speed and buoyancy profiles need to be obtained, which we assume to happen either from using a database like that of Levitus, or by measurement in the region and time of interest. In addition to these two profiles, two parameters must be provided: the strength of the internal-wave spectrum (ζ_o^2) and the F factor. It therefore becomes of interest to have a systematic view of these two parameters as a function of geography and geophysical time (season, month, or whatever is relevant to possible changes in these two parameters).

We have very little information about variations in ζ_o^2 as a function of time or space. The best we can do at present is use one number (the reference level) or refer to very specific experiments. For example, the SLICE89 experiment in the North Pacific between California and Hawaii in 1989 measured a ζ_o^2 of about 25 m^2[13], while preliminary results from the ATOC experiment in a nearby region in 1997 give about 100 m^2 (Kevin Heaney, private communication, 1997). The GM75 reference level of 50 m^2 was observed in a nearby region in 1974 by several experiments. Thus variations of a factor

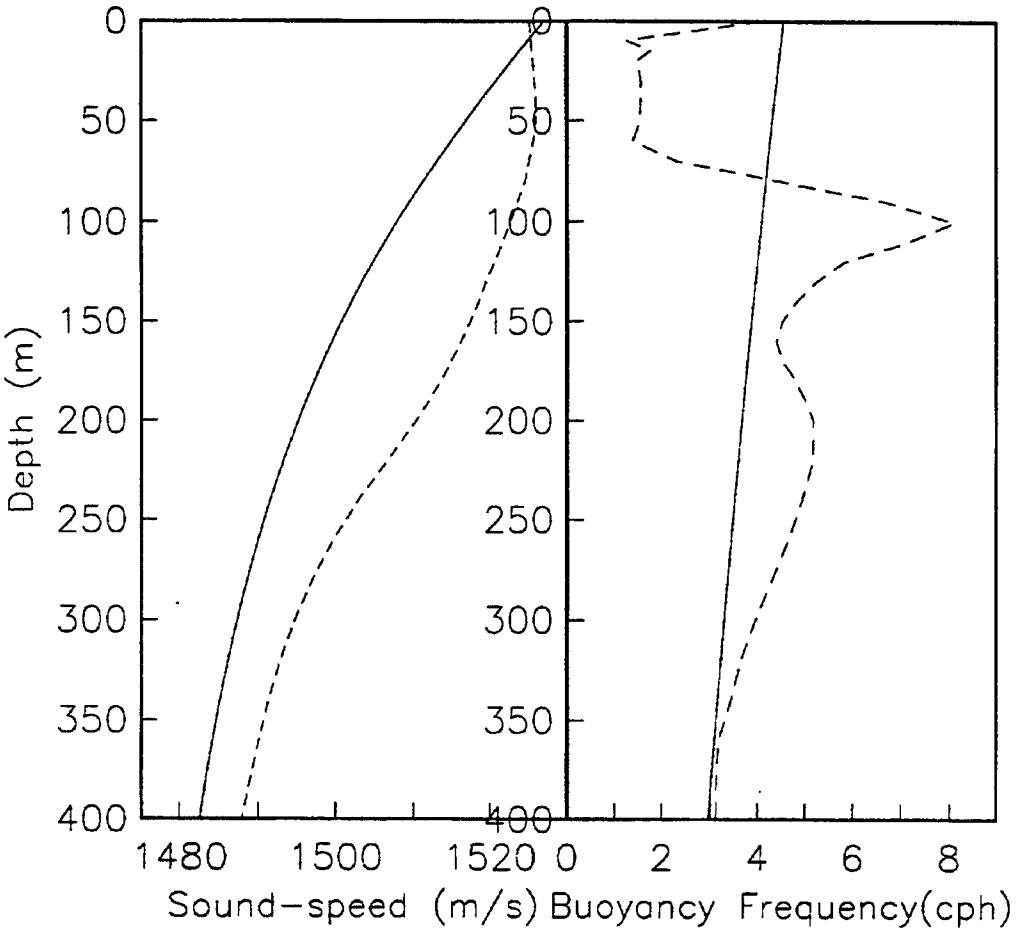

Figure 10: The profiles of sound speed and buoyancy frequency, for the average of a set of profiles observed in the ocean between California and Hawaii (dashed), and for a canonical profile used in simulations of the SLICE89 experiment (solid).

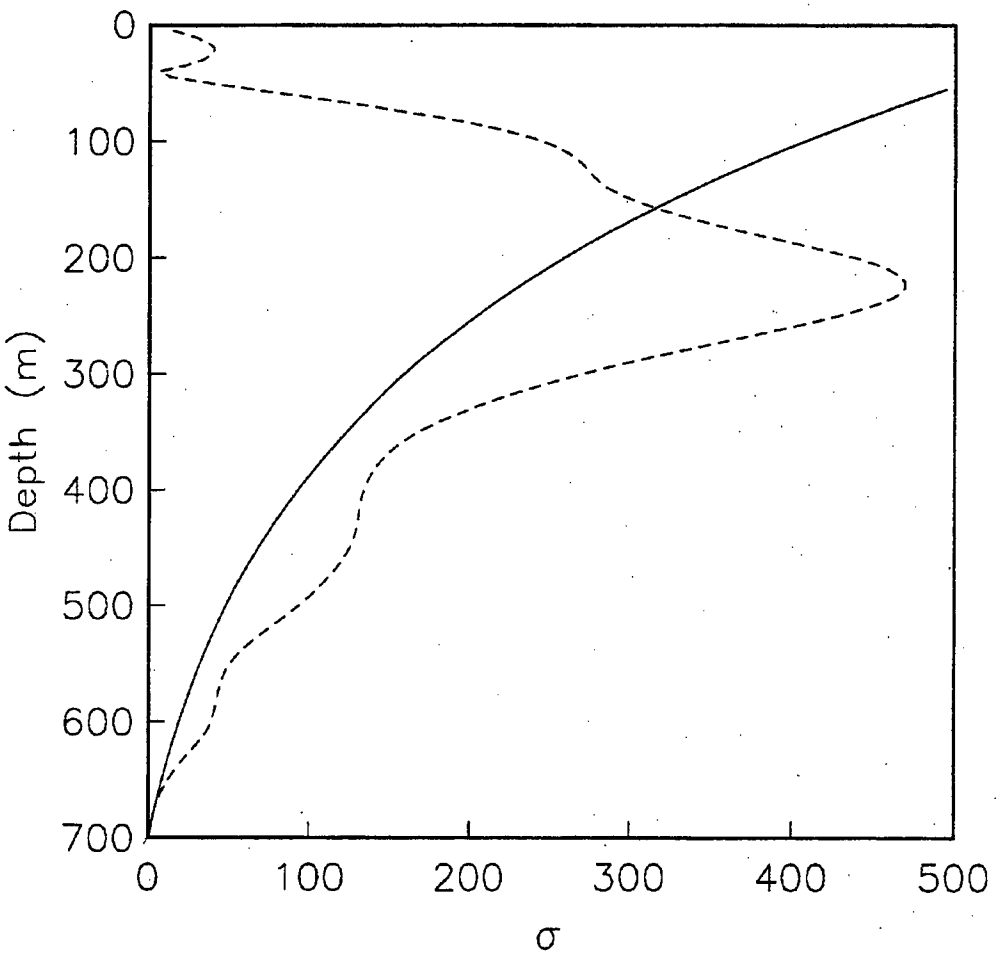

Figure 11: The profiles of σ for the two sets of profiles shown in the previous figure.

of four with different geophysical time have been observed in an ocean-basin sized region. These experiments varied in their spatial averaging from a few kilometers to 5 megameters.

The variation of F with time may be assumed to be small for depths deeper than 300 m, and thus a single map of F can be created. Figure 12 shows such a map created from the previous plots in this study. A temperature of 10° C has been chosen as representative of depths of interest. The value of F varies by a factor of three, although in temperate latitudes the variation is considerably less.

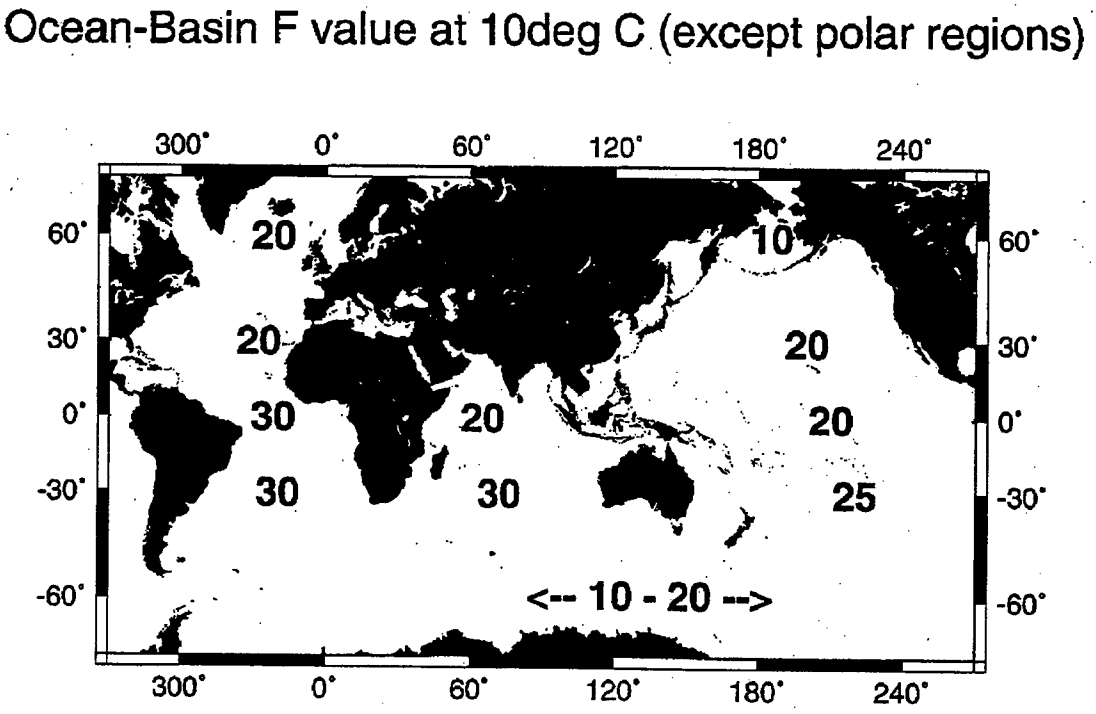

Figure 12: Geographical distribution of F at a temperature of 10° C.

3 ACOUSTIC SIGNAL-GAIN ESTIMATES

Calculations of acoustic fluctuations have been carried out by means of formulas derived by use of path-integral techniques.[5, 14, 15] These formulas comprise numerical integrals along rays from a source. These rays could be characterized in various ways; in this study we have used a source at 500-m depth in order to obtain rays whose upper turning points (UTP) span the region between the surface and 500-m depth. It has been found that the variation with UTP depth can be substantial; however, we will pick a single number that characterizes an acoustic fluctuation quantity without worrying too much about UTP-depth dependence of the result.

Calculations have been made for ranges of 500 km and 2000 km. The results scale with range according to relatively simple expectations, so that extrapolations to other ranges are not difficult. Therefore we can present the results only for 500 km and refer to scaling to obtain results at other ranges.

Calculations have been made for twelve ocean regions. We have studied the equatorial regions as a function of latitude, and have used values between 5° and 10° to avoid the singularity at 0°.

Five acoustic fluctuation quantities have been calculated. Each is expressed in a form that is independent of acoustic frequency to first approximation. However, the sonar-system designer and operator are of course interested in dependences on acoustic frequency, which will be discussed.

Each quantity is calculated separately for each ray. The actual acoustic field at the receiver will be a sum of rays: deterministic multipath. The combination of rays implied by a given source-receiver geometry is assumed to be a solvable signal-processing problem.

Each quantity and its implications on sonar-system design and operation are described below:

- critical frequency f_c - The implication of τ is mainly in controlling the upper limit on frequencies for which internal-wave effects are negligible. Taking a simple rule-of-thumb that wavefront fluctuations less than $\lambda/10$ are negligible, the critical frequency can be calculated from the rms travel-time fluctuation τ. Thus, $f_c = 100/\tau$ where f_c is in Hz and τ is in ms. For example, if $\tau = 4$ ms, then frequencies below 25 Hz have negligible internal-wave effects. Conversely, internal-wave effects for frequencies above 25 Hz will be non-negligible.

- coherent bandwidth *cbw* - Incoherence between frequencies can be translated into the time domain as the spread of an individual pulse during transmission. Considering that the width of a pulse is about twice the rms spread τ_0, the coherent bandwidth can be calculated from the rms spread as $cbw = 500/\tau_0$ where *cbw* is in Hz and τ_0 is in ms. For example, a 4-ms rms spread translates into a coherent bandwidth of 125 Hz.

- coherence time t_0, expressed in acoustic periods - The coherence time is controlled by the motion of internal waves, and it controls the maximum integration time that can be used for coherent temporal integration. For example, a coherence time of 40,000 periods at 100 Hz translates to 400 seconds coherent integration time.

- vertical coherence length l_v, expressed in acoustic wavelengths - The vertical coherence length controls the maximum length that can be used for coherent spatial integration. In the vertical, plane-wave beamformers are not adequate; complete models of the propagation to form a "matched field" must be done, but the principle is the same; the signal gain available from a vertical aperture is approximately the vertical aperture in wavelengths, sot he signal gain in the vertical is l_v. Note that in the case of shallow water, the water depth may be less than the

physical length represented by l_v; in that case the water depth in units of acoustic wavelengths replaces l_v.

- horizontal coherence length l_h, expressed in acoustic wavelengths - The horizontal coherence length is in principle even simpler than the vertical, because plane waves are a good approximation in the horizontal. Thus the signal gain in the horizontal is l_h.

A two-dimensional, billboard array that takes advantage of both vertical and horizontal aperture will be able to achieve a signal gain (SG) against isotropic noise of $l_v l_h$. The final result of our calculations will be a plot of SG versus range for a variety of ocean regions, assuming specific values of F and ζ_o^2. The sonar-system designer can use this information to incorporate limits resulting from internal-wave effects into a design. The sonar-system operator, with local information about F and ζ_o^2, can predict whether an operating system will be impeded strongly by internal waves or not.

In particular, given the same sound-speed profile, each of the acoustic fluctuation quantities listed above are inversely proportional to a factor Q, where:

$$Q = F \cdot [n(z)]^2 \cdot \zeta_{rms} \tag{3-1}$$

Note that the factor is ζ_{rms}, not ζ_0. The local internal-wave displacement ζ_{rms} does depend on $n(z)$, but it is more direct to use the local displacement in order to more easily use experimental results. A systematic example of this is the assumption we will make that ζ_{rms} is about the same in shallow water as in deep, while the buoyancy frequency $n(z)$ is typically a factor of two larger in shallow water than in deep.

In deep water, signal gain is inversely proportional to Q^2, because each of l_v and l_h yield one power of Q. In shallow water, the vertical factor is missing, giving only one power of Q.

3.1 Definition of Ray and Ray-Tube Geometries

It is useful to describe the sound speed in the ocean as:[5]

$$c(\vec{s}) \;=\; c_o[1 + U(z) + \mu(\vec{s})] \tag{3-2}$$

where c_o is the axial (minimum) sound speed, $U(z)$ is a function of vertical position only and represents the deterministic sound channel, and $\mu(\vec{s})$ is the zero-mean fractional sound-speed variation caused by internal waves.

$$\partial_{xx}[z_{ray}(x)] = -\frac{1}{c(z)}\partial_z[c(z)] \tag{3-3}$$

The trajectory of a ray in the ocean sound channel, where z is the depth and x is the range, satisfies the Eikonal equation. Rather than define many variables, we give the parabolic approximation to that equation with a range-independent sound speed $c(z)$, since it will lead to simpler raytube functions later:

Because we are using a geometrical-optics basis for our calculations, the Green's function takes the form of ray-tube behavior.[5] Figure 13 shows a curved ray from a source to a receiver with definitions of two ray-tube functions ξ_1 and ξ_2. These functions of range between source and receiver begin with value zero and end with value unity. The difference between them is that ξ_1 begins at the source and ξ_2 begins at the receiver. Each of the ξ functions satisfy the raytube equation:

$$\partial_{xx}\xi(x) + U''[z_{ray}(x)]\xi(x) \;=\; 0 \tag{3-4}$$

Later, a function $S_1(x)$ will appear in some of the expressions for acoustic fluctuation quantities; it is the solution of Equation (3-4) with initial conditions $S_1(0) = 0$ and $S_1'(x) = 1$.. where U'' is the second derivative of $U(z)$.

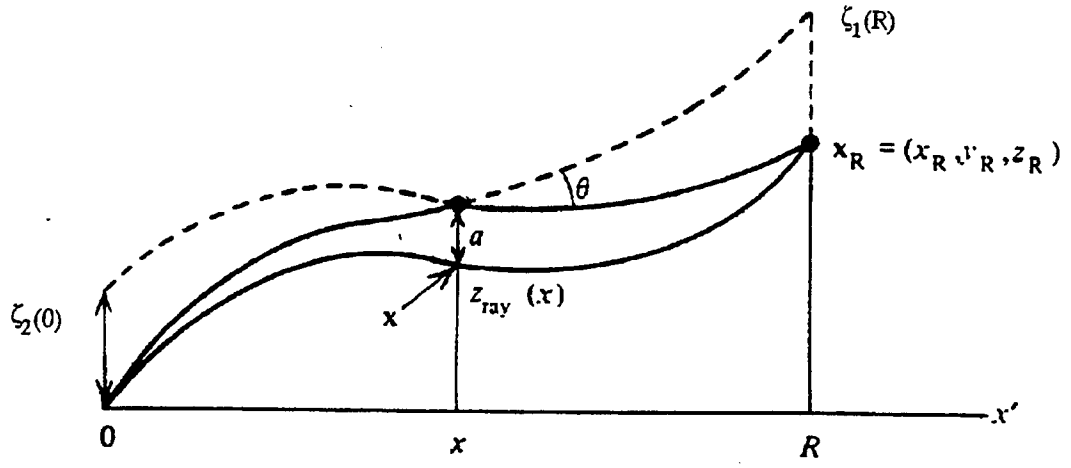

Figure 13: Ray and raytube definitions. The function ξ_1 starts from zero at the source and has a value of unity at the receiver. The function ξ_2 is zero at the receiver and unity at the source. These two functions represent the difference between two rays launched from the source or receiver with infinitesimally different launch angles.

3.2 Acoustic Fluctuation Quantities

In the following, the acoustic frequency will be denoted by σ_a. (The logarithmic dependence of *cbw*, l_v, and l_h on acoustic frequency is weak; we have used 100 Hz for σ_a to evaluate these expressions.)

Various quantities averaged over the internal-wave spectrum will be denoted by {quantity}. Detailed expressions for these averages are given in Flatté and Stoughton.[15]

3.2.1 f_c (critical frequency for significant internal-wave effects)

Expressions for f_c are obtained from its relation to τ, the rms travel-time

fluctuation:

$$f_c = \frac{100}{\tau} \tag{3-5}$$

where f_c is in Hz and τ is in ms. The quantity τ is given by:

$$\tau^2 = \frac{1}{C_o^2} \int_0^R dx \langle \mu^2 \rangle L_p \tag{3-6}$$

3.2.2 *cbw* (coherent bandwidth)

The coherent bandwidth is obtained from its relation to τ_0, the rms pulse spread;

$$cbw = \frac{500}{\tau_0} \tag{3-7}$$

where *cbw* is in Hz and τ_0 is in ms.

The quantity τ_0 is given by:

$$\begin{aligned} \tau_0^2 &= \frac{1}{2}[\frac{\ln(\sigma_a \tau)}{C_o} S_1(R)]^2 \int_0^R dx \langle \mu^2 \rangle L_p\{k_v^2\} \\ &\cdot \int_0^R dx' \langle (\mu')^2 \rangle L_p'\{k_v'^2\} [\xi_1(x)\xi_2(x')]^2 \end{aligned} \tag{3-8}$$

3.2.3 t_o (coherence time in periods)

The quantity t_0 is given by:

$$t_0^{-2} = [\frac{2\pi \ln \sigma_a \tau}{C_o}]^2 \int_0^R dx \langle \mu^2 \rangle L_p\{\omega^2\} \tag{3-9}$$

3.2.4 l_v (vertical coherence length in wavelengths)

The quantity l_v is given by:

$$l_v^{-2} = [\ln(\sigma_a \tau)]^2 \int_0^R dx \langle \mu^2 \rangle L_p \{k_v^2\} [\xi_1(x)]^2 \tag{3-10}$$

3.2.5 l_h (horizontal coherence length in wavelengths)

The quantity l_h is given by a rather complicated formula, because of the complicated nature of the internal-wave spectrum as a function of horizontal wavenumber components.[15]

$$l_h^{-2} = [\frac{4}{L_{p0}^3 \Delta y}]^2 \int_0^R dx \langle \mu^2 \rangle L_p [\frac{x}{R}]^{3/2} [1 + \rho_s^2]^{3/4} \tag{3-11}$$

where Δy is a reference horizontal separation. The calculations here have been done with Δy set to 1 km; note that the dependence of l_h on Δy is quite weak.

3.3 Calculational Results for Acoustic Fluctuation Quantities

Table 3 shows the results for calculations of the five acoustic fluctuation quantities, as described above. Some systematic behavior may be noted:

- Very different sound-speed profiles in high-latitude areas result in the critical frequencies being significantly higher there.
- The behavior of the acoustic propagation in polar regions where there is usually no sound channel results in significantly lower coherent band-

Table 3: Acoustic fluctuation quantities for 500-km range through a reference-level internal-wave field. The units are: Hz for the critical frequency f_c (below which internal-wave effects are negligible) and the coherent bandwidth cbw; kiloperiods for the coherence time t_0; and wavelengths for the coherence lengths l_v and l_h.

Ocean Region	f_c	cbw	t_0	l_v	l_h
NPA	100	25	250	300	14000
NPP	14	10	250	150	2500
NA	25	500	90	600	3000
NP	16	250	60	500	2000
EA	20	500	180	1000	1700
EP	20	500	200	800	1700
EI	16	500	200	600	1700
SA	20	170	90	600	3000
SP	20	170	80	600	3000
SI	20	700	80	600	3000
SPA	70	50	100	200	8000
SPI	50	17	150	200	8000

width at those frequencies for which internal-wave effects are not negligible.

- Temperate-latitude regions are reasonably similar to each other.
- Equatorial regions have larger coherence times, larger vertical coherence lengths, and smaller horizontal coherence lengths than nearby temperate regions.

3.4 Billboard Signal Gains for Different Conditions (SG vs R)

By use of the values of l_h and l_v from Table 3, the signal gain (SG) against isotropic noise can be calculated. The coherence lengths to a good approximation scale as the square root of the range. The signal gain is the

product of two coherence lengths, so it scales linearly with range. This scaling is reasonable as long as one remains in deep water. As one moves into shallow water two modifications need to be made.

- The value of ζ will be assumed to stay constant, while the value of $n(z)$ increases by a factor of two. By use of Equation (3-1), the horizontal coherence length will decrease by a factor of four below its value extrapolated from deep water. This will decrease the signal gain by 6 dB.
- The vertical coherence length extrapolated from deep water will be replaced by the water depth. To represent shallow water, a depth of 200 m will be used to calculate SG. This gives a different correction for each ocean region, but the typical correction is a reduction in SG of 20 dB.

Values of SG for different ocean regions as a function of range are shown in Figure 14. The shallow-water point has been chosen to be 20 km, and the ranges between 20 and 500 km have been filled in by a smooth curve, not by any precise calculation.

Achievement of these maximal signal gains would require the development of billboard acoustic arrays that are tens of kilometers wide and span the ocean water column in depth. Hundreds of thousands of hydrophones in each array would be necessary. Nevertheless, these are the ocean limits.

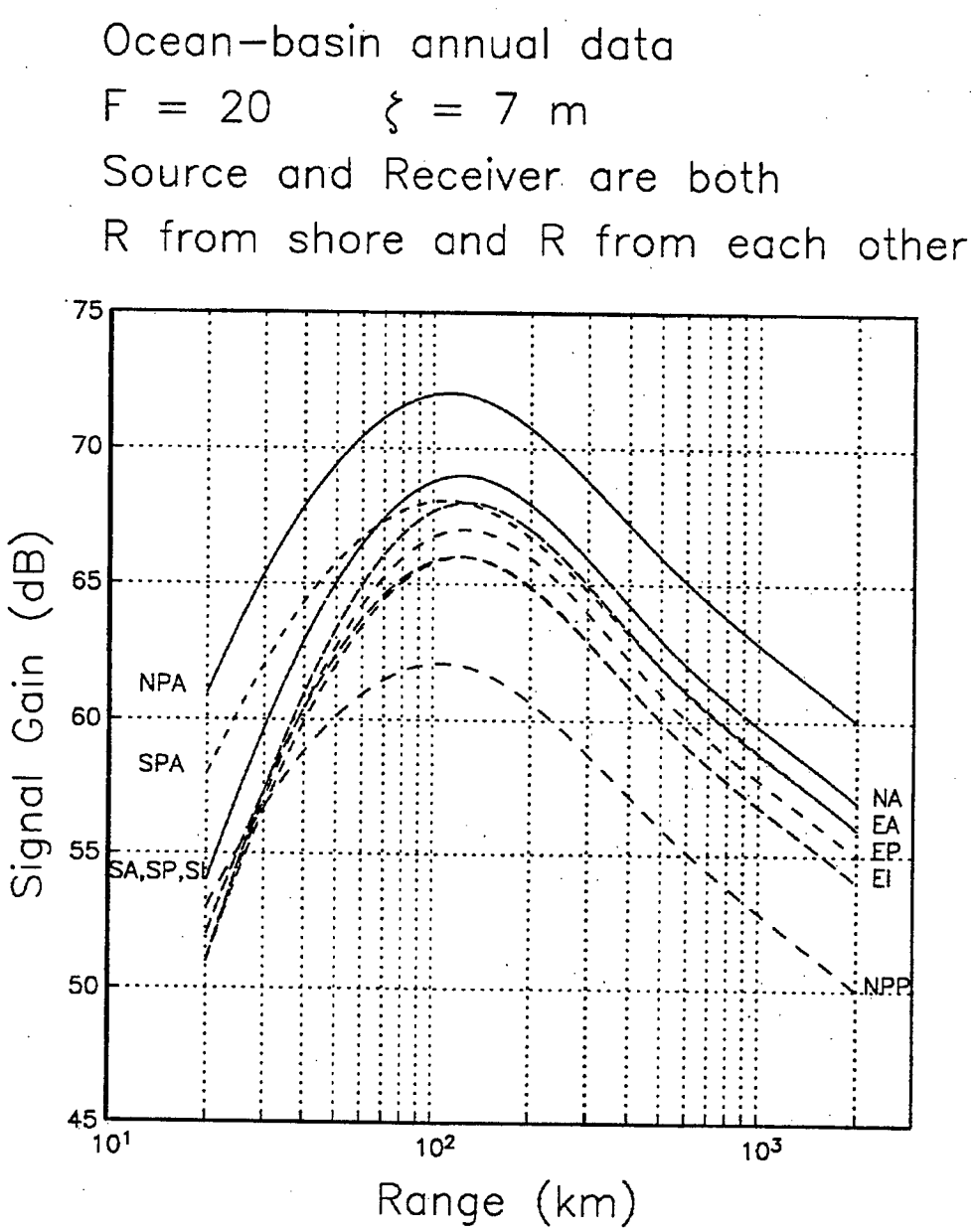

Figure 14: Limits due to a reference-level internal-wave field ($\zeta_o^2 = 50$ m^2; $F = 20$) for signal gain against isotropic noise for a billboard array. Vertical and horizontal apertures are set to the coherence lengths due to internal waves. Results are shown for different ocean regions as a function of range between source and receiver. The short ranges are assumed to be in shallow water as explained in the text. (In deep water the maximum signal gain is inversely proportional to range.)

4 RECOMMENDATIONS

This study has combined present oceanographic knowledge of the temperature-salinity structure in the sea with knowledge of the effects of internal waves on acoustic propagation. It has been revealed that two parameters are of paramount importance to the understanding of internal-wave effects on sonar systems: the local strength of the internal-wave field and the local value of a factor F that represents the ratio of fractional variations in sound-speed and density. The F factor has been oceanographically studied in the form of temperature salinity relationships, and reasonable values for many, but not all, ocean regions are available. The variation of internal-wave strength is known to be substantial, but no systematic information is available at the present time on which to base designs of sonar systems.

If the behavior of sonar systems in conditions in which they are limited by internal waves is desired, the following recommendations are strongly suggested:

- Initiate a substantial monitoring program to follow the strength of internal waves as a function of season and ocean region.
- Validate and make more precise the use of the F factor described in this report.
- Develop an appropriate generalization of the GM spectrum that is valid across the equator.
- Verify the validity of the use of the GM spectrum in shallow water, or replace it with a new systematic model.

ACKNOWLEDGMENTS

Thanks are due to Kimberly Noble and Galina Rovner for help in making calculations and plots.

References

[1] W. Munk and C. Garrett, "Internal waves in the ocean," Ann. Rev. Fluid Mech. **11,** 339–369 (1979).

[2] S. Flatté and R. Esswein, "Calculation of the phase-structure function density from oceanic internal waves," J. Acoust. Soc. Am. **70,** 1387–96 (1981).

[3] C. Chen and F. Millero, "Precise equation of state of seawater for oceanic ranges of salinity, temperature, and pressure," Deep Sea Research **24,** 365–369 (1977).

[4] V. D. Grosso, "New equation for the speed of sound in natural waters (with comparisons to other equations)," J. Acoust. Soc. Am. **56,** 1084–1091 (1974).

[5] S. Flatté, R. Dashen, W. Munk, K. Watson, and F. Zachariasen, *Sound Transmission through a fluctuating Ocean* (Cambridge University Press, Cambridge, 1979).

[6] J. Apel, L. Ostrovsky, and Y. Stepanyante, "Internal solitons in the ocean," APL/JHU Report MERCJRA0695, Applied Physics Laboratory-Johns Hopkins University (1995) .

[7] R. H. Headrick, Ph.D. thesis, Massachussetts Institute of Technology-Woods Hole Oceanographic Institution, Woods Hole, Massachussetts, 1997.

[8] S. Flatté and G. Rovner, "Path-integral expressions for fluctuations in acoustic transmissions in the ocean waveguide," In *Proceedings of the 1997 'Aha Huliko'a Workshop on Physics and Oceanography,* P. Muller, ed., p. in press (Univ. of Hawaii, 1997).

[9] W. H. Munk, "Sound channel in an exponentially stratified ocean, with application to SOFAR," J. Acoust. Soc. Am. **55,** 220–226 (1974).

[10] W. H. Munk and F. Zachariasen, "Sound propagation through a fluctuating stratified ocean: Theory and observation," J. Acoust. Soc. Am. **59,** 818–838 (1976).

[11] J. Colosi, S. Flatté, and C. Bracher, "Internal-wave effects on 1000-km oceanic acoustic pulse propagation: Simulation and comparison with experiment," J. Acoust. Soc. Am. **96,** 452–68 (1994).

[12] W. Munk, P. Worcester, and C. Wunsch, *Ocean acoustic tomography* (Cambridge University Press, London, 1995).

[13] T. F. Duda, S. M. Flatté, J. A. Colosi, B. D. Cornuelle, J. A. Hildebrand, W. S. Hodgekiss, P. F. Worcester, B. M. Howe, J. A. Mercer, and R. C. Spindel, "Measured wave-front fluctuations in 1000-km pulse propagation in the Pacific Ocean," J. Acoust. Soc. Am. **92(2),** 939–955 (1992).

[14] S. M. Flatté, "Wave propagation through random media: Contributions from ocean acoustics," Proc. of the IEEE **71,** 1267–1294 (1983).

[15] S. M. Flatté and R. B. Stoughton, "Predictions of internal-wave effects on ocean acoustic coherence, travel-time variance, and intensity moments for very long-range propagation," J. Acoust. Soc. Am. **84,** 1414–1424 (1988).

DISTRIBUTION LIST

Director of Space and SDI Programs
SAF/AQSC
1060 Air Force Pentagon
Washington, DC 20330-1060

CMDR & Program Executive Officer
U S Army/CSSD-ZA
Strategic Defense Command
PO Box 15280
Arlington, VA 22215-0150

Superintendent
Code 1424
Attn Documents Librarian
Naval Postgraduate School
Monterey, CA93943

DTIC [2]
8725 John Jay Kingman Road
Suite 0944
Fort Belvoir,VA 22060-6218

Dr. A. Michael Andrews
Director of Technology
SARD-TT
Room 3E480
Research Development Acquisition
103 Army Pentagon
Washington, DC 20301-0103

Dr. Albert Brandenstein
Chief Scientist
Office of Nat'l Drug Control Policy
Executive Office of the President
Washington, DC 20500

Dr. H. Lee Buchanan, III
Deputy Director
DARPA/DSO
3701 North Fairfax Drive
Arlington, VA 22203-1714

Dr. Collier
Chief Scientist
U S Army Strategic Defense Command
PO Box 15280
Arlington, VA 22215-0280

D A R P A Library
3701 North Fairfax Drive
Arlington, VA 22209-2308

Dr. Victor Demarines, Jr.
President and Chief Exec Officer
The MITRE Corporation
A210
202 Burlington Road
Bedford,MA01730-1420

Mr. Frank Fernandez
Director
DARPA/DIRO
3701 North Fairfax Drive
Arlington, VA 22203-1714

Mr. Dan Flynn [5]
Deputy Chief
OSWR
CDT/OWTP
4P07, NHB
Washington, DC 20505

Dr. Paris Genalis
Deputy Director
OUSD(A&T)/S&TS/NW
The Pentagon, Room 3D1048
Washington, DC 20301

Dr. Lawrence K. Gershwin
NIO/S&T
2E42, OHB
Washington, DC 20505

Mr. David Havlik
Manager
Weapons Program Coordination Office
MS 9006
Sandia National Laboratories
PO Box 969
Livermore, CA94551-0969

Dr. Helmut Hellwig
Deputy Asst Secretary
(Science, Technology and Engineering)
SAF/AQR
1060 Air Force Pentagon
Washington, DC 20330-1060

Dr. Robert G. Henderson
Director
JASON Program Office
The MITRE Corporation
1820 Dolley Madison Blvd
Mailstop W553
McLean, VA 22102

DISTRIBUTION LIST

J A S O N Library [5]
The MITRE Corporation
Mail Stop W002
1820 Dolley Madison Blvd
McLean, VA 22102

Mr. O' Dean P. Judd
Los Alamos National Laboratory
Mailstop F650
Los Alamos, NM 87545

Dr. Bobby R. Junker
Office of Naval Research
Code 111
800 North Quincy Street
Arlington, VA 22217

Dr. Martha Krebs
Director
Energy Research, ER-1, Rm 7B-058
1000 Independence Ave, SW
Washington, DC 20858

Dr. Ken Kress
Investment Program Office (IPO)
1041 Electric Avenue
Vienna,VA 20180

Lt Gen, Howard W. Leaf, (Retired)
Director, Test and Evaluation
HQ USAF/TE
1650 Air Force Pentagon
Washington, DC 20330-1650

Dr. John Lyons
Director of Corporate Laboratory
US Army Laboratory Command
2800 Powder Mill Road
Adelphi,MD 20783-1145

Dr. Arthur Manfredi
ZETA Associates
10300 Eaton Drive
Suite 500
FairfaxVA 22030-2239

Dr. George Mayer
Scientific Director
Army Research Office
4015 Wilson Blvd
Tower 3, Suite 216
Arlington, VA 22203-2529

Ms. M. Jill Mcmaster
Editor
Journal of Intelligence Communication
Investment Program Office (IPO)
1041 Electric Avenue
Vienna,VA 20180

Dr. Bill Murphy
ORD
Washington, DC 20505

Dr. Julian C. Nall
Institute for Defense Analyses
1801 North Beauregard Street
Alexandria, VA 22311

Dr. Ari Patrinos [5]
Associate Director for
Biological and Environmental Reserach
ER-70
US Department of Energy
19901 Germantown Road
Germantown,MD 207874-1290

Dr. Bruce Pierce
USD(A)D S
The Pentagon, Room 3D136
Washington, DC 20301-3090

Mr. John Rausch [2]
Division Head 06 Department
NAVOPINTCEN
4301 Suitland Road
Washington, DC 20390

Records Resource
The MITRE Corporation
Mailstop W115
1820 Dolley Madison Blvd
McLean,VA 22102

Dr. Victor H Reis [5]
US Department of Energy
DP-2, Room 4A019
Mailstop 4A-028
1000 Independence Ave, SW
Washington, DC 20585

Dr. Fred E. Saalfeld
Director
Office of Naval Research
800 North Quincy Street
Arlington, VA 22217-5000

DISTRIBUTION LIST

Dr. Dan Schuresko
O/DDS&T
OSA/ATG
Room 23F20N, WF-2
Washington, DC 20505

Dr. John Schuster
Submarine Warfare Division
Submarine, Security & Tech
Head (N875)
2000 Navy Pentagon Room 4D534
Washington, DC 20350-2000

Dr. Michael A. Stroscio
US Army Research Office
P. O. Box 12211
Research Triangle Park,NC27709-2211

Ambassador James Sweeney
Chief Science Advisor
USACDA
320 21st Street NW
Washington, DC 20451

Dr. George W. Ullrich [3]
Deputy Director
Defense Special Weapons Agency
6801 Telegraph Road
Alexandria, VA 22310

Dr. David Whelan
Director
DARPA/TTO
3701 North Fairfax Drive
Arlington, VA 22203-1714

Dr. Edward C. Whitman
US Naval Observatory
Nval Oceanographers Office
3450 Massachusetts Ave, NW
Washington, DC 20392-5421